JOURNAL OF GEOPHYSICAL RESEARCH: BIOGEOSCIENCES, VOL. 118, 1–14, doi:10.1002/jgrg.20043, 2013

The ecohydrology of forested peatlands: Simulating the effects of tree shading on moss evaporation and species composition

N. Kettridge,[1] D. K. Thompson,[2,3] L. Bombonato,[4] M. R. Turetsky,[5]
B. W. Benscoter,[6] and J. M. Waddington[2]

Received 21 September 2012; revised 17 January 2013; accepted 22 February 2013.

[1] Forested peatlands represent an important global carbon pool, storing 48.0 Pg of carbon within continental western Canada alone. Peatland hydrology regulates the carbon dynamics and future stability of this carbon store and provides a critical control on regional water dynamics. Drying associated with land-use change and climate change has the potential to increase tree growth, modifying the density, size, and spatial arrangement of trees. This can reduce peatland evaporation and offset the associated increase in transpiration. To determine the magnitude of this negative ecohydrological feedback, we simulated spatial variations in radiation, turbulent energy fluxes, and temperatures in peatlands with real and idealized tree densities and distributions. For a random tree distribution, an increase in tree density from 0 to 4 trees per m^2 reduced available energy at the peat surface, decreasing average evaporation by 25%. At higher tree densities, feather moss species covered a larger fraction of the ground because of lower light availability. In combination with the lower energy availability, this change in moss composition reduced evaporation by ~70%. The reduction in evaporation was greater (83%) when the effects of increased canopy cover on peatland aerodynamic properties were incorporated. Additionally, we found that evaporation was dependent on the spatial arrangement of trees, with evaporation being higher when trees were clustered. Overall, our model showed that the trade-off between reduced evaporation and increased transpiration with increasing tree densities reduced landscape variation in evapotranspiration, with simulated evapotranspiration remaining approximately constant across a broad range of peatland ecosystems despite varying canopy densities.

Citation: Kettridge, N., D. K. Thompson, L. Bombonato, M. R. Turetsky, B. W. Benscoter and J. M. Waddington (2013), The ecohydrology of forested peatlands: Simulating the effects of tree shading on moss evaporation and species composition, *J. Geophys. Res. Biogeosci.*, *118*, doi:10.1002/jgrg.20043.

1. Introduction

[2] The hydrological response of northern peatlands to changing climatic conditions, and the vulnerability of their large carbon stocks [*Turunen et al.*, 2002; *Tarnocai et al.*, 2009], is controlled by a complex array of interconnected ecohydrological feedback mechanisms [*Belyea*, 2009; *Morris et al.*, 2012] that operate across a range of temporal scales. Feedback mechanisms that regulate peatland water loss over short (daily to annual) or long (millennial) time scales have received recent attention. For example, studies recently have documented the controls of peat moisture content on evaporation losses [*Bond-lamberty et al.*, 2011], and the control of decomposition on rates and patterns of ground water flow [*Baird et al.*, 2012]. However, the control of medium-term (decadal) ecohydrological feedback mechanisms, associated principally with shifts in plant communities and population densities within northern peatlands [*Strack et al.*, 2006], has received little attention and provides a considerable knowledge gap in our understanding of the vulnerability of these global carbon stores to land-use change and changing climate conditions.

[3] Ombrotrophic peatlands across the subhumid boreal plain and shield of western Canada are dominated by an open black spruce canopy [*Rowe*, 1959; *Ecoregions Working Group*, 1989]. Hydrological disturbance has the potential to increase tree growth, modifying the density, size, and spatial arrangement of these trees [*MacDonald and Yin*, 1999], providing an important feedback response to drying. Although it may be assumed that evapotranspiration losses will increase as a result of tree growth, it has been suggested that trees can

[1]School of Geography, Earth and Environmental Sciences, University of Birmingham, Edgbaston, Birmingham, UK.
[2]McMaster Centre for Climate Change and School of Geography and Earth Sciences, McMaster University, Hamilton, Ontario, Canada.
[3]Natural Resources Canada, Canadian Forest Service, Edmonton, Alberta, Canada.
[4]Department of Biology and Evolution, University of Ferrara, Ferrara, Italy.
[5]Department of Integrative Biology, University of Guelph, Guelph, Ontario, Canada.
[6]Department of Biological Sciences, Florida Atlantic University, Davie, Florida, USA.

Corresponding author: N. Kettridge, School of Geography, Earth and Environmental Sciences, University of Birmingham, Edgbaston, Birmingham, B15 2TT, UK. (n.kettridge@bham.ac.uk)

2169-8961/13/10.1002/jgrg.20043

strengthen the water conserving function of the peatland landscape [*Thompson*, 2012] by reducing the available energy for moss evaporation. Subcanopy evaporation provides an important [*Heijmans et al*., 2004], if not dominant, component of the evapotranspiration flux from forested peatlands [*Lafleur and Schreader*, 1994; *Thompson*, 2012]. Transpiration is often limited by the low stem densities within the peatland [*Wieder et al*., 2009] and the adverse impact of waterlogged, nutrient-poor peatland ecosystem on black spruce transpiration [*Lieffers and MacDonald*, 1990]. In comparison, evaporation is maximized by the large proportion of solar radiation reaching the wet subcanopy because of the low stem density and the narrow structure of the black spruce canopy. Increased transpiration rates associated with a higher black spruce stem density may therefore be insufficient to counteract reductions in subcanopy evaporation that result from reduced energy availability at the peat surface. However, the magnitude and form of this potentially important ecohydrological feedback mechanism is unknown.

[4] The effect on evaporation (E; kg m^{-2}) of trees shading the peat surface from direct and diffuse radiation cannot be considered in isolation. An increasing tree density induces a range of additional feedback mechanisms that regulate evaporative losses under a changing canopy density. Peat evaporation is often modeled using a form of the Penman-Monteith equation, e.g.,

$$E = \frac{s(T_s - T_a) + vdd_a}{R_a + R_s}, \quad (1)$$

where T_s and T_a are the surface and air temperatures (K), respectively, s is the slope of the saturation vapor versus temperature curve (kg m^{-3} K^{-1}), vdd_a is the vapor density deficit of air (kg m^{-3}), R_a is the aerodynamic resistance (s m^{-1}), and R_s is the surface resistance (s m^{-1}) [*Oke*, 1987]. The surface resistance accounts for water being held under tension (negative water potential) within the near surface peat [*Philips*, 1957], and the aerodynamic resistance accounts for the resistance to the turbulent transport of water vapor through the surface boundary [*Kettridge and Baird*, 2006]. Both the surface resistance and the aerodynamic resistance may be modified significantly by a changing vegetation canopy, providing important additional feedback to evaporative losses.

[5] Surface resistance to evaporation in peat depends strongly on the rate of evapotranspiration [*McCarter and Price*, 2012]. If water supply through the peat profile is unable to meet evapotranspirative losses, tensions within the near surface increase and evaporation is reduced. An increased evaporative demand within a peatland with a lower tree density, therefore, may be counteracted by an increased surface resistance producing only a small increase in water loss (although high surface resistance may also be introduced by the increased transpiration rates that will lower near-surface moisture contents). The surface resistance to evaporation also varies significantly between different subcanopy vegetation. Most notably, feather moss has a higher surface resistance to evaporation than *Sphagnum* species [*Brown et al*., 2010] and as a result is better able to retain water within the peatland. Variations in the density or spatial arrangement of trees will modify the available light within the subcanopy, impacting the understory species. Feather moss generally out-competes *Sphagnum* under low light conditions when the sky view factor is less than ~20% [*Bisbee et al*., 2001]. Thus, under low light conditions with a low evaporative demand, the subcanopy will be dominated by feather moss species, further limiting evaporative losses.

[6] Variations in the density and spatial arrangement of trees also impact the aerodynamic properties of the subsurface, modifying the aerodynamic resistance to evaporation. The addition of trees to a treeless peatland landscape substantially increases the aerodynamic roughness of the surface, reducing the aerodynamic resistance and increasing evaporation. For example, the surface roughness of a treeless poor fen within Sweden and a treed fen in central Alberta, Canada were equal to 0.02 m [*Mölder and Kellner*, 2002] and 0.22 m [*Thompson*, 2012], respectively. Although a further increase in tree density produces a smoother aerodynamic surface as the tree canopy fills in, reducing surface roughness, this also raises the displacement height (equal to zero within a treeless peatland [*Mölder and Kellner*, 2002]), increasing the resistance from the canopy sublayer to the evaporation surface [*Niu and Yang*, 2004].

2. Aim and Objectives of Research

[7] This research aims to examine the stability of the peatland hydrology to increased tree densities. We hypothesize that if short-term simulations demonstrate an increased evapotranspiration under higher tree densities, additional feedback mechanisms will be required to limit water loss from the peatland and to control the resultant drop in the water table position. The magnitude of this drop will depend on the strength of these feedback mechanisms (not examined here). We used field and lab studies to examine the following specific research objectives:

[8] 1. To quantify how evaporation differs between peatlands with varying tree densities.

[9] 2. To determine the extent to which differences in evaporation result from reduced energy availability at the peat surface, a transition in the subcanopy vegetation under reduced light conditions, or a modification to the aerodynamic properties of the peat surface.

[10] 3. To ascertain the extent to which the spatial organization of trees within the peatland (notably clustering) impacts the rate of evaporation.

[11] 4. To identify the extent to which any reduction in evaporation is counteracted by an increase in tree transpiration under higher tree densities.

[12] These objectives are critical to understand the medium-term response of peatlands to disturbance. In this study, we aimed to apply our new understanding to examine the functioning of peatlands at discrete stages along the succession gradient observed in space for time studies, e.g., post wildfire [*Wieder et al*., 2009]. However, we did not attempt to understand how individual ecosystems develop continuously through time nor did we examine how tree growth, hydrology, and chemistry interact.

3. Methods

3.1. Boreal Ecohydrology Tree Algorithm Model Development

[13] We developed a new Boreal Ecohydrology Tree Algorithm (BETA) model that simulates the surface energy exchanges, subcanopy ecology, and subsurface peatland thermal behavior in three dimensions within a forested boreal peatland. The model is principally a unification of the HIP-3D model [*Kettridge and Baird*, 2010] and the tree radiative transfer model of *Essery et al*. [2008]. Details of the modeling approach are provided within *Kettridge and Baird* [2010, 2008] and *Essery et al*. [2008] and so are not repeated in detail here. Instead, here we provide an overview of the modeling framework. The separate modeling components that make up BETA have each been evaluated successfully individually within the literature; notably the evaluation of the HIP-3D model [*Kettridge and Baird*, 2010] and the radiative transfer model of *Essery et al*. [2008]. BETA therefore does not provide new processes-based information. Rather, BETA integrates previously evaluated process-based knowledge into a single modeling framework. This allows interactions and feedbacks between the different, previously isolated, model components, enabling a broader examination of the ecosystem iterations and function.

[14] The Boreal Ecohydrology Tree Algorithm is a dynamic model that simulates evaporation from forested peatlands at a high temporal resolution (time step = 30 s), driven from standard micrometeorological data (air temperature, humidity, incoming short wave radiation). Horizontal and vertical transfers of energy and water are calculated in accordance with HIP-3D, a finite difference model in which the peatland is discretized in three dimensions. Energy transfers occur in accordance with Fourier's law. The surface moisture content is assumed to be in hydrostatic equilibrium with the water table depth and the moisture content profile calculated in accordance within the modified capillary rise model of *Kettridge and Baird* [2007]. To compare evaporation rates between different peatland with varying tree densities, model simulations are performed here over short time periods (two days). Only the impact of changing atmospheric properties is examined (variations in net radiation and atmospheric turbulence). Therefore, the subsurface hydrology is kept constant between the different peatlands. Model simulations are thus performed with a defined static water table position (at a depth of 0.15 m). The location of trees across the peat surface are defined within BETA either from field measurements (see section 3.2) or from the statistical tree generation model (outlined below). In accordance with *Essery et al*. [2008], trees are assumed to have ellipsoidal canopies and cylindrical trunks to enable the analytical calculation of the path lengths of rays of light through the canopy (l_t). Tree shape and size are defined by the tree height (H_{top}; m), canopy radius (r_c; m), and trunk radius (r_t; m; Figure 1).

[15] The measured above canopy incoming short-wave radiation is separated into its direct and diffuse fractions in accordance with HIP-3D; based on the difference in the short-wave radiation between the measured above canopy value and its calculated optimal cloud free value [*Brock and Arnold*, 2000]. For a given time during daylight hours,

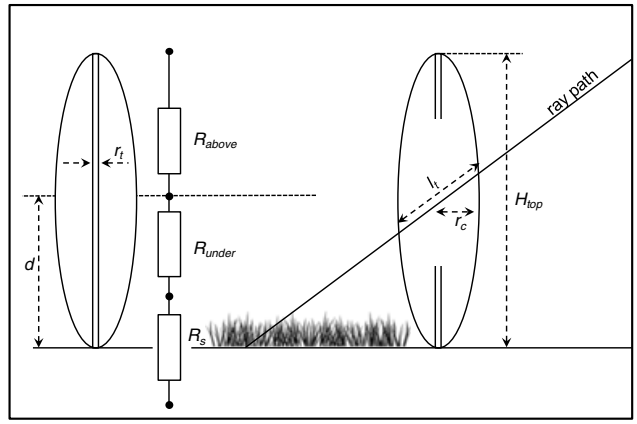

Figure 1. Schematic diagram of the BETA model surface boundary, adapted from *Essery et al*. [2008].

each point on the discretized surface is either in direct radiation or in the shadow of the tree canopy (direct radiation equals zero). The shading of the ground surface from the direct radiation is calculated in accordance with *Essery et al*. [2008]. The path of a ray of light travelling from each node on the discretized peat surface in the direction of the Sun is determined and the total path length through tree canopies and tree trunks calculated [*Essery et al*., 2008]. The transmissivity of tree trunks is equal to zero. If the ray path at a specific location and time travels through a tree trunk then the direct radiation at that location is equal to zero (it is in the shade). The probability of the ray of light passing through the tree canopy (p_c) is dependent on the path length through the canopy, the canopy foliage area volume density, and the arrangement of the canopy elements (i.e., clumping within the canopy). Within the radiative transfer model of *Essery et al*. [2008], p_c was assumed to decrease exponentially with path length, calculated from

$$p_c = e^{-G(\theta)\sum \lambda l_t}, \tag{2}$$

where λ is the foliage area volume density (m^{-1}) and G is the projection function, accounting for the orientation of the canopy elements (−), the latter being a function of the solar elevation (θ). Equation (2) is parameterized within section 3.2 below.

[16] The diffuse fraction of incoming short-wave radiation from the sky is assumed to be isotropic and, therefore, the fraction reaching the subcanopy at a given location and time is equal to the product of the above canopy diffuse radiation and the sky view factor; the observable proportion of the sky from a given location of the peat surface. The sky view factor at a given point is calculated in accordance with *Essery et al*. [2008], by numerical integration of values of p_c in all directions within the visible hemisphere. The transmission of direct and diffuse radiation through the subcanopy shrub layer to the peat surface is calculated using Beer's law [*Kettridge and Baird*, 2008] assuming a uniform leaf area index of 0.5.

[17] Net long-wave radiation is calculated in accordance with HIP-3D, with the sky view factor of the canopy and subcanopy equal to that of the diffuse faction of the incoming short-wave radiation. Evaporation and the sensible heat flux are calculated from the Penman-Monteith equation and

Newton's law of cooling [cf. *Kettridge and Baird*, 2008]. The surface resistance is constant and is dependent on the vegetation species at the ground surface (see vegetation submodel) and the aerodynamic resistance is dependent on the tree canopy (see aerodynamic resistance submodel). Both the vegetation and aerodynamic submodels can be turned on and off to investigate model function and behavior.

3.1.1. Vegetation Submodel

[18] The surface moss species at each position within the BETA model is determined from the calculated sky view factor. In accordance with *Bisbee et al*. [2001], the probability of a specific location being *Sphagnum*, as opposed to feather moss (p_s) is

$$p_s = \frac{e^{-3.46+1379 \cdot vf}}{1 + e^{-3.46+1379 \cdot vf}}, \quad (3)$$

where vf (−) is the view factor. If the vegetation submodel is turned off, the subcanopy is assumed to be composed entirely of *Sphagnum*. The surface resistance of the *Sphagnum* and feather moss are calculated from chamber measurements of evapotranspiration (see section 3.2).

3.1.2. Aerodynamic Resistance Submodel

[19] The aerodynamic resistance is the sum of two components: the aerodynamic resistance above and below the canopy sublayer (Figure 1). The aerodynamic resistance above the subcanopy (R_{above}) is calculated in accordance with the HIP-3D model. However, unlike HIP-3D, the displacement height (d) and the roughness length of momentum of the canopy (z_{0m}) vary with the canopy density. The roughness length of momentum of the canopy is equal to $0.13(H_{\text{top}} - d)$ in accordance with *Abtew et al*. [1989]. For a canopy cover less than 0.7, d is the product of the geometric mean canopy height (H_{top}) and canopy cover (C) [*Abtew et al*., 1989]. For a canopy cover greater than 0.7, d is equal to $0.7H_{\text{top}}$ [*Cionco*, 1983].

[20] The resistance from under the canopy sublayer (R_{under}) is calculated in accordance with *Niu and Yang* [2004]

$$R_{\text{under}} = \frac{H_{\text{top}}}{aK_h(H_{\text{top}})}\left[e^{a\left(1-z_{0g}/H_{\text{top}}\right)} - e^{a\left(1-(z_{0m}+d)/H_{\text{top}}\right)}\right], \quad (4)$$

where H_{top} is the canopy height (m), z_{0g} the ground roughness length (m), equal to the surface roughness of a treeless peatland [$z_{0g} = 0.02$ m; *Mölder and Kellner*, 2002]. The absorption coefficient of momentum, a (−), is equal to

$$a = \left(\frac{c_d H_{\text{top}} LSAI}{l_m}\right)^{0.5}, \quad (5)$$

under the assumed neutral stability conditions, where c_{d} is the drag coefficient of the canopy (−), l_{m} is the mean mixing length (m) and LSAI is the leaf and steam area index (−) [*Niu and Yang*, 2004]. For a coniferous tree, $c_{\text{d}} = 0.2$ and $l_{\text{m}} = 1.13$ m [*Goudriaan*, 1977]. The eddy diffusivity K_h (H_{top}) ($\text{m}^2\ \text{s}^{-1}$) for heat at the top of the canopy is equal to

$$K_h(H_{\text{top}}) = \kappa u_*(H_{\text{top}} - d), \quad (6)$$

where κ is the von Karman constant (−) and u^* is the friction velocity (m s^{-1}) [*Niu and Yang*, 2004]. LSAI is calculated from the tree canopy volume multiplied by the trees foliage area volume, λ. λ averaged $3.87 \pm 1.7\ \text{m}^{-1}$ and was calculated from the product of the dry foliage mass of 48 trees [cf. *Johnston*, 2012] and the specific leaf area of black spruce ($5.82\ \text{m}^2\ \text{kg}^{-1}$) [*Bond-Lamberty et al*., 2002], divided by the canopy volume (calculated from tree height; section 3.2). If the vegetation submodel is turned off, R_{above} is calculated with defined values of d and z_0 (equal to 0 m and 0.36 m), and R_{under} is equal to zero.

3.1.3. Statistical Tree Generation

[21] A simple statistical model is developed in BETA to generate artificial tree distributions with varying spatial statistics. The model produces a broad range of trees with different tree densities and different spatial organizations. The model does not aim to replicate either the specific processes of tree generation nor provide an exact representation tree spatial organization within given peatlands. The statistical model produces a defined number or trees within the study area, equal to n_{tree}. First, a number of trees (n_{primary}) are randomly distributed throughout the study area. Second, successive trees are added from these initial trees. A primary tree is selected at random, and a successive tree is added in a random direction at a stochastic distance from the primary tree. The distance of this tree from the primary tree is assumed to follow a folded normal distribution, with a mean equal to zero and defined standard deviation, σ. A buffer distance of 0.2 m is added to this stochastically calculated distance, restricting generation of the successive tree in extremely close proximity to the primary tree. Subsequently, a random tree is selected from either the primary trees or the previously located successive trees. The processes of locating a new secondary tree is then repeated as above. This process is repeated until the number of trees within the study area equals n_{tree}. To produce spatially organized trees, the number of primary trees are varied between 1 and 19, and σ between, and 0.3 and 3.3 m. Example tree locations are presented in Figure 2. To generate a random distribution of trees, the number of trees within the simulation is equal to the number of primary trees.

[22] The attributes of each tree (tree height, canopy radius, trunk radius, canopy transmissivity) are assumed independent of the tree location and formation; i.e., whether the tree is defined as a primary or successive tree, or the iteration number of the tree in the generation sequence. Tree height is assumed to follow a log-normal distribution, with a mean and standard deviation defined from field measurements. Trunk radius follows a stochastic linear relationship with tree height, while canopy radius and transmissivity are an independent stochastic function, each calculated from field measurements.

3.2. Model Parameterization

3.2.1. Tree Shape, Size, and Transmissivity

[23] Tree metrics (shape, size and transmissivity) were calculated within a 30 × 30 m area of Athabasca bog (54.72°N 113.17°W), a small forested bog approximately 7 km east of Athabasca, Alberta, Canada. The tree canopy is characterized by *Picea mariana*, with a total of 388 trees within the experimental area (equivalent to 4311 stems per ha). Tree age within the bog range between 28–32 years in ~2004, suggesting the last fire at the bog occurred approximately 45 to 50 years previously [*Benscoter et al*., 2005]. The location of trees within the study showed no clear spatial organization, with clustered areas within the central and northwestern sections of the study area, and areas with a more uniform distribution to the south and the east

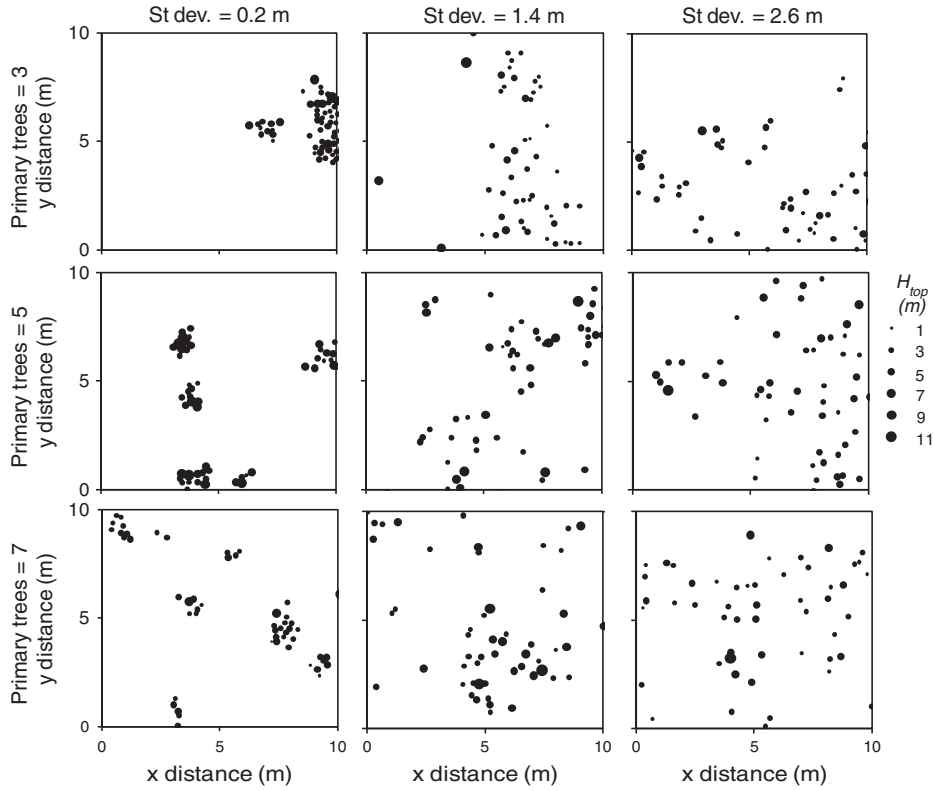

Figure 2. Example of tree sizes and locations generated from the statistical tree generation model. Columns from left to right represent increases in the standard deviation of the generated tree locations from primary trees and rows represent the number of primary trees.

(Figure 3). Clustering of the trees was analyzed using Moran's *I*, comparing the average nearest neighbor distance, the distance between each tree within the study plot and its nearest neighbor, to that of a hypothetical random distribution.

[24] The radius of the tree trunk was measured at the base of each tree within the study area. In addition, a total of 104 trees within the western proportion of the study area were photographed to determine tree height, canopy radius, and transmissivity. A photograph was taken of the side of each tree with an orange backdrop and scale erected behind and adjacent to the tree, respectively. Each pixel within the photographs was classified as either tree or nontree within ImageJ [*Schneider et al*., 2012] and an ellipse drawn, which best represented the tree shape. The tree height and tree radius were equal to the height and radius of the ellipse in the scaled image. To quantify canopy transmissivity, a 3-D ellipsoid was generated from the ellipse (how the tree would be represented within BETA) and the horizontal path length through the ellipsoid calculated for each pixel. Each pixel thus has a defined path length and a binary value for whether or not the light passed directly through the tree (whether or not the pixel was classified as tree). Path lengths, excluding those that travelled through the tree trunk, were classified into 0.01 m bins. The probability of a ray of light travelling horizontally through the tree was calculated for each bin, equal to the proportion of pixels within each bin not classified as tree. BETA assumes that p_c is independent of the ray path direction through the canopy, and is thus equal to the values calculated for horizontal ray paths.

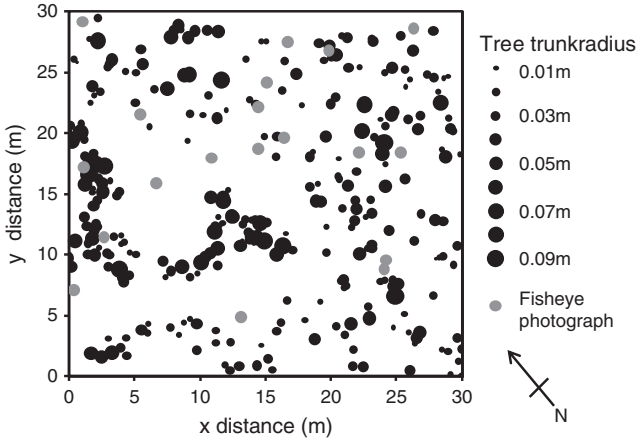

Figure 3. Location of fisheye photographs and trees, with associated tree trunk radius, within the 30 × 30 m plot.

3.2.2. Subcanopy Surface Resistance

[25] The effect of tree shading on peatland evaporation rates was determined at Burnt Crow Bog (55.81°N 115.11°W), a forested *P. mariana* bog located ~80 km north of Slave Lake, Alberta, Canada. The site last burnt in 1935 and has a current tree density of 16,000 stems per hectare. *Sphagnum* species, primarily *S. fuscum*, dominate the peat surface. However, areas of feather moss (particularly *Pleurozium schreberi*) are present, generally within lower light regions. In the summer of 2010, 20 plots, 10 controls (C), and 10 treatments (T), were identified within Burnt

Crow Bog. Of these 20 plots, 10 were dominated by *P. mariana* and feather mosses and the other 10 were dominated by *P. mariana* and *S. fuscum*. Following a several week baseline observation period, trees were cut and removed within the treatment plots on 17 June 2010 resulting in five plots each of: controls, trees, and feather moss (CF); controls, trees, and *S. fuscum* (CS); treatment, trees removed, and feather moss (TF); treatment, trees removed, and *S. fuscum* (TS). The sky view factor of each plot was measured from fisheye photography, in accordance with section 3.3, within each plot both prior to and after the removal of the tree canopy.

[26] Evaporation rates were measured once a week using the approach outlined by *McLeod et al*. [2004]. A PVC collar was installed at each plot on 25 May 2010. Collars (0.03 m^2, 10 cm deep) were positioned in areas with a homogeneous cover of *Sphagnum fuscum* (CS and TS) or feather moss (CF and TF). A Perspex chamber was placed over each collar for 2 min and the increase in chamber humidity measured every 1.6 s using a PP Systems EGM-4 infrared gas analyzer. The evaporation rate was calculated from the linear change in vapor density during the first minute of measurement. Changes in vapor concentration leveled off considerably after 1 min due to a decrease in the vapor gradient across the peat-air interface. Measurements were obtained between 10:00 and 16:00 to minimize flux variations caused by the diurnal cycle.

[27] The instantaneous rate of evapotranspiration (ET_{in}; mm h^{-1}) was calculated from the slope of vapor density within the chamber [*Stannard*, 1988]

$$ET_{\text{in}} = 3.6\left(\frac{MVC}{A}\right), \tag{8}$$

where M is the rate of increase in vapor density within the chamber during the measurement (g m^{-3} s^{-1}), V is the volume inside the chamber (m^3), C is the calibration factor to account for vapor absorption within the chamber (dimensionless) and A is the area of ground surface covered by the chamber (m^2). The conversion factor of 3.6 was used in order to convert a volume of water per unit area (g H_2O m^{-2} s^{-1}) into an hourly flux rate (mm h^{-1}). Surface resistance (s m^{-1}) was derived from observations of instantaneous surface evapotranspiration in m s^{-1} [*van de Griend and Owe*, 1994; *Daamen and Simmonds*, 1996]

$$R_s = \frac{\rho_s^* - \rho}{ET_{\text{in}}} - R_a, \tag{9}$$

where ρ and ρ_s* are the observed and saturated vapor density, respectively (kg m^{-3}), and R_a is the aerodynamic resistance of the chamber used for ET_{in} (kg m^{-2} s^{-1}) measurement, which was equal to 50 s m^{-1} in this case.

[28] The control of treatment (*Sphagnum* control, *Sphagnum* tree removed, feather moss control, feather moss tree removed) on evapotranspiration and surface resistance were analyzed using a general linear model in SAS (Proc GLM) with treatment as a fixed effect and collar ID as a random effect to account for lack of independence among repeated collar measurements. We used least significant difference tests for post hoc comparison of means.

3.3. Sky View Factor Evaluation

[29] Boreal Ecohydrology Tree Algorithm provides an integration of previously evaluated models to determine the impact of interactions between different ecosystem processes on peatland evaporation. However, one component of BETA has been modified from the previous model evaluations. The light transmission properties of the radiative transfer model of *Essery et al*. [2008] has been modified to represent the black spruce trees found within the peatlands of the boreal plain. The radiation component of the model is therefore evaluated to determine whether this new parameterization provides an adequate characterization of the incoming radiation at the peat surface within a peatland with a sparse tree density. Hemispherical photographs were taken across the 30 × 30 m study area at a total of 26 locations with a range of surrounding tree densities (Figure 3). Photographs were taken using a Nikon D60 camera and a Sunex 185° Super Fisheye lens. At each location, the camera was placed on a leveled tripod just above the peat surface and the photographs taken skyward. Photographs were processed using Gap Light Analyser [*Frazer et al*., 2001] to calculate the sky view factor.

[30] The sky view component of BETA was evaluated by comparing the observed sky view factors to sky view factors simulated by BETA. Ten realizations of BETA were performed to calculate the simulated sky view factor at each location. Within these simulations, tree locations and tree trunk radii were parameterized based on field measurements (Figure 3). H_{top} was calculated from a linear relationship with the measured tree trunk radius. Canopy radius and transmissivity were assumed independent of the tree location and size, and were randomly determined for each tree from normal distributions, with the mean and standard deviation calculated from the subset of 104 trees.

3.4. Model Simulations

[31] Forward simulations of BETA were conducted in two formats: with a random tree distribution and with spatially organized tree distributions determined from the statistical tree generation model. The random tree distribution model was applied to investigate the impact of tree density on peatland evaporation, examining the affect of differences in tree shading, *Sphagnum*-feather moss cover and aerodynamic roughness. Simulations were performed within a 10 × 10 m area, with a 2 m buffer zone (demonstrated to provide similar results to a 40 m buffer; data not shown). Two hundred simulations were performed with the number of trees within the 10 × 10 m area increasing from 1 to 400 (from 100 to 40,000 stems ha^{-1}). This covered the range of tree densities observed by *Wieder et al*. [2009] across a fire chronosequence, ranging from 0.3 to 3.7 trees per m^{-2}. Tree locations varied between each simulation in addition to the tree heights, canopy radii, tree radii, and canopy transmissivities, which were randomly determined for each tree from the observed distributions. Simulations were initially performed with the vegetation and aerodynamic resistance submodels turned off and then repeated with the vegetation submodel turn on and the aerodynamic submodel turn off. Simulations were then conducted with both the vegetation and aerodynamic submodel turned on. Simulations were driven from measured micrometeorological data (air temperature, incoming short wave radiation, humidity) obtained from burnt crow, a raised forested ombrotrophic peatland complex in central Alberta, Canada (55.8°N, 115.1°W); see *Kettridge et al*. [2012] for site description. Driving micrometeorological data were obtained between 00:00 on 15 July and 00:00 on 17 July 2010.

[32] The statistical tree generation model was applied to determine the effect of tree spatial organization on peatland evaporation. Simulations were performed at three tree densities, with 50, 150, and 250 trees within the 10 × 10 m area (5000, 10,000 and 15,000 stems per ha). For each tree density, a total of 100 simulations were performed with the standard deviation and primary tree number ranging from 1 to 19, and 0.2 to 2.9 m, respectively. The different primary tree numbers and standard deviations impacted the spatial organization of the trees at the given densities (see Statistical Tree Generation section).

3.5. Tree Transpiration Model

[33] A simple tree transpiration model was developed to identify whether the simulated decreases in the evaporation from the subcanopy were substantial enough to counteract the projected increases in transpiration associated with an increasing tree density. Tree transpiration (T; mm d^{-1}) is calculated from

$$T = A_{tb} E_{st} VPD \tag{10}$$

where A_{tb} is the tree basal area per m^2 (−), VPD is the average daytime vapor pressure deficit (kPa) [*Oren et al.*, 1996], and E_{st} is the sapwood transpiration efficiency (mm d^{-1} kPa^{-1}). Tree transpiration is assumed independent of the water table position. E_{st} is estimated as 782 mm d^{-1} kPa^{-1}, calculated from sapwood sensors [*Thompson*, 2012]. We do not take account here of the effect of increasing tree density on interception losses.

4. Results

4.1. Tree Parameterization

[34] Canopy height demonstrated an approximately log-normal distribution; average log canopy height equal to 0.44 ± 0.15 m (Figure 4b). Canopy radius was normally distributed, averaging 0.36 ± 0.14 m (Figure 4a). Although canopy radius was significantly correlated with H_{top}, the explanatory component of this relationship was low ($p = 0.002$; $r^2 = 0.08$). Canopy radius was thus assumed independent of H_{top} within BETA simulations. Tree trunk radius ranged between 0.0025 and 0.04 m and was significantly correlated with H_{top} ($r^2 = 0.77$; $p > 0.01$; Figure 5).

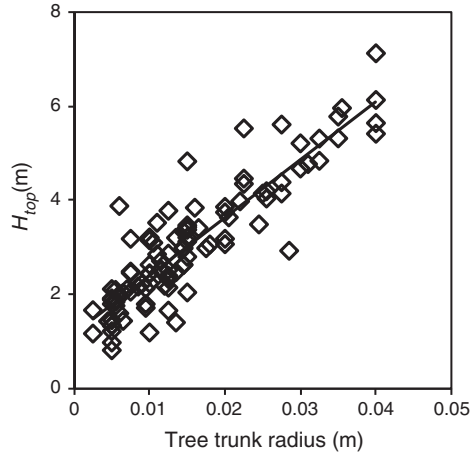

Figure 5. Relationship between tree trunk radius (r_{tree}) and H_{top}. The solid black line represents the results of a linear regression model ($H_{top} = 123 r_{tree} + 1.16$, $r^2 = 0.80$, $p < 0.001$, $F = 395$).

[35] The probability of a ray of light travelling through the tree canopy did not demonstrate a clear exponential relationship with the canopy path length (equation (2) and Figure 6a). This results from the nonuniform nature of the foliage area volume density within the black spruce tree. Foliage density is much higher within the central proportion of the tree. As a result, p_c is dependent on the distance from the measurement location to the tree center, normalized by the canopy radius (Figure 6b). To improve simulations of p_c for given path lengths through the tree canopy, developments are required that take this behavior into account. However, for this initial application of the BETA model, we apply the exponential relationship, which best approximates the magnitude of the probability p_c for given path lengths (Figure 6a).

4.2. Subcanopy Parameterization

[36] Prior to tree removal, field measurements showed that the sky view factor did not differ either between the control (0.60 ± 0.08) and treatment (0.65 ± 0.09) plots ($p > 0.05$, $t = -1.58$) or between the *Sphagnum* (0.60 ± 0.06) and feather moss (0.64 ± 0.11) plots ($p > 0.05$, $t = -1.16$). Following tree removal, the sky view factor was significantly higher in the

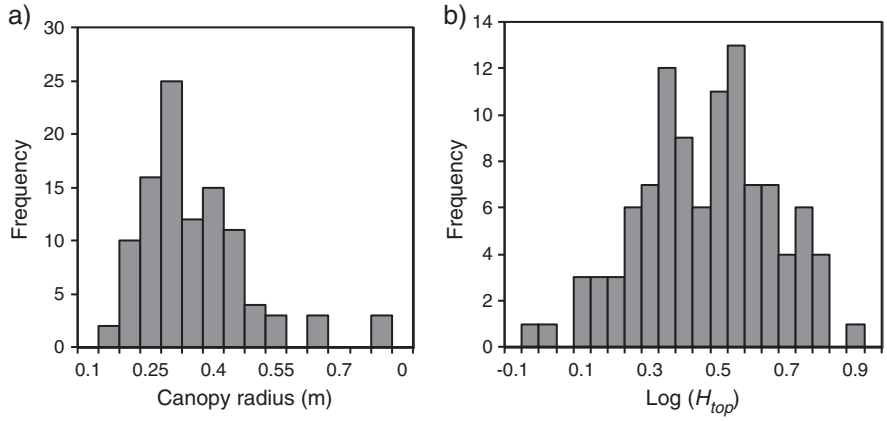

Figure 4. Frequency of (a) canopy radius and (b) log (H_{top}).

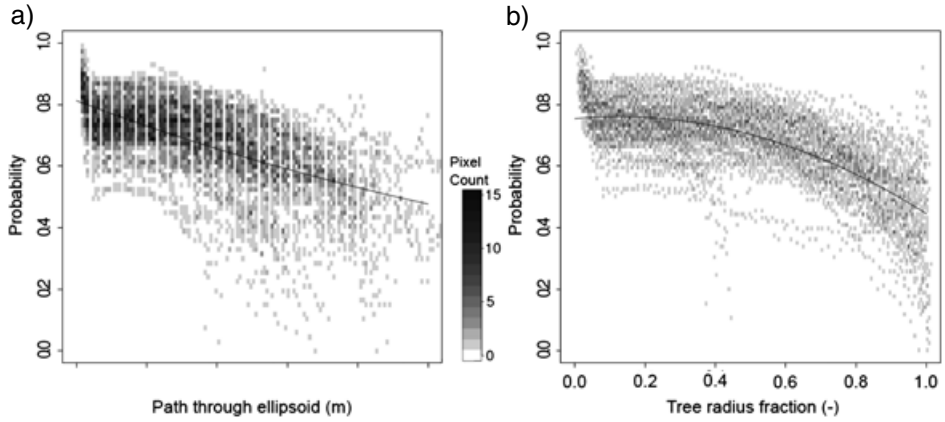

Figure 6. Probability of a ray of light passing horizontally through the tree for (a) a given path length through the ellipsoid and (b) the distance from the edge of the tree through which the ray of light travelled, expressed as a fraction of the tree radius (where 0 equals the tree edge and 1 equals the center of the tree). Due to the high density of points, data are presented as the number of points per pixel.

treatment plots (0.85 ± 0.03) relative to the control plots (0.60 ± 0.08) ($p < 0.001$, $t = -9.7$). There was a significant treatment effect on rates of evapotranspiration ($p < 0.001$, $F_{3,16} = 30.75$), indicative of an interaction between groundcover vegetation and tree removal. Collar ID was not a significant random effect in our model ($p = 0.44$, $F_{3,16} = 1.0$). Averaged across tree removal treatments, ET in *Sphagnum* plots was higher than in feather moss plots (0.28 ± 0.003 mm h^{-1} versus 0.12 ± 0.001 mm h^{-1}) ($p < 0.001$; $t = 2.1$). For *Sphagnum* dominated plots, ET was higher in the plots with trees removed (0.46 ± 0.2 mm h^{-1}) than the control plots (0.35 ± 0.15 mm h^{-1}; Figure 7). Therewere no differences in ET between the feather moss control and tree removal plots, which overall averaged 0.24 ± 0.14 mm h^{-1}. Surface resistance also varied significantly among treatments ($p < 0.001$, $F_{3,16} = 25.99$), but this was controlled by vegetation differences rather than the effects of tree removal. Collar was a significant random effect in our model ($p = 0.02$). Surface resistance of feather moss treatment and control plots did not differ from one another. Averaged across treatment and control plots, feather moss surface resistance averaged 484 ± 223 s m^{-1}; which was higher than any of our *Sphagnum* plots. The *Sphagnum* treatment and control plots also did not vary from one another, and resistance averaged 118 ± 79 s m^{-1}.

4.3. Sky View Factor Validation

[37] Simulated view factors within Athabasca bog vary between zero and 0.94 (Figure 8). Values equal to zero are isolated and associated with trees being located on simulation nodes. Simulated sky view factors of ~0.30 are the minimum widely observable values within the study area. The impact of tree spatial organization on sky view factors can be clearly identified, with areas of the peatland with a high clustering of trees representing a strong contrast in sky view factors. In comparison, regions with more dispersed organization of trees show a more uniform sky view factor. The BETA model provides a reasonable approximation of the magnitude of the sky view factors (Figure 9), with an RMS error of 0.15. This, in combination with the previous evaluation of the radiation component of the BETA model

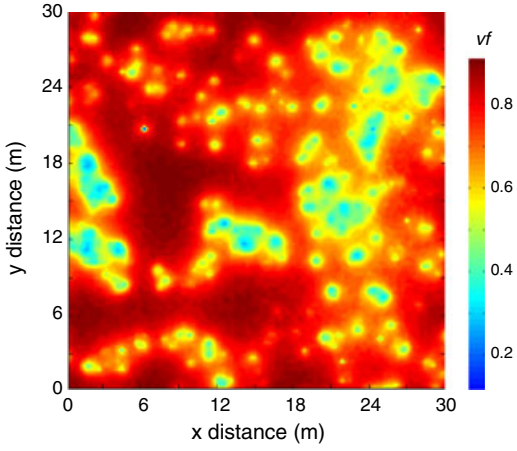

Figure 7. Average evaporation rates within the Burnt Crow study plots; trees and feather moss (CF); trees and *S. fuscum* (CS); trees removed and feather moss (TF); trees removed and *S. fuscum* (TS). Dotted line indicates the onset of our experimental tree removal in the field.

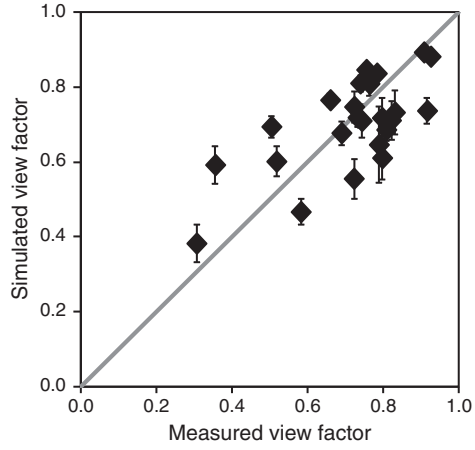

Figure 8. Spatial variation in the simulated sky view factors within the 30 × 30 m study area at Athabasca bog; shown in plan view.

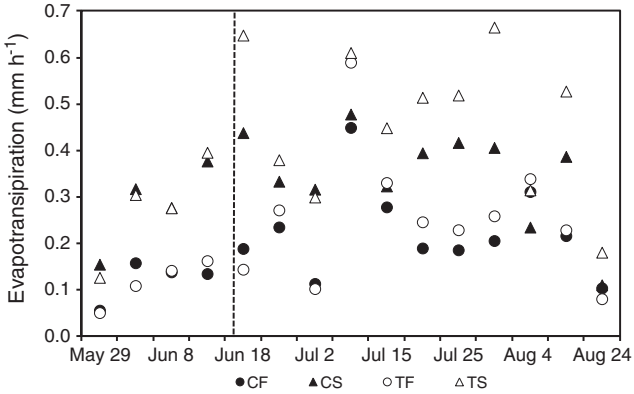

Figure 9. Simulated and measured view factors within the 30 × 30 m study period at Athabasca bog. The line represents the 1:1 relationship (RMS error of 0.15).

[*Essery et al*., 2008], strongly suggests the model will provide a reasonable approximation of the short- and long-wave radiation at the peat surface, which provides a key control on the magnitude of evaporation.

4.4. Model Simulation: Random Tree Distribution

[38] Tree density provides an important control on the simulated latent heat flux. With the aerodynamic and vegetation submodels turned off, differences in simulated latent heat flux result from variations in the available energy at the peat surface. Under these conditions, the latent heat flux decreases almost linearly with an increasing tree density; by 25% between a tree density of 0 and 4 trees per m^2 (Figure 10a). Turning the vegetation submodel on produces a further, strongly nonlinear, reduction in latent heat flux with increasing tree density (Figure 10a). Between a tree density of 0 and 0.5 trees per m^2, the decrease in latent heat flux associated with the vegetation submodel is small; light levels across all but the most shaded regions of the subcanopy are high enough for *Sphagnum* to outcompete feather moss. As the tree density increases, *Sphagnum* growth is strongly limited by available light and feather moss begins to out-compete *Sphagnum*, increasing the surface resistance to evaporation (Figure 10b; surface resistance). This transition from *Sphagnum* to feather moss occurs principally between a density of 1 to 2.5 trees per m^2 and it is between this range that the latent heat flux shows the greatest reduction. Above a tree density of 2.5 trees per m^2, the subcanopy is dominated by feather moss and further reductions in the latent heat flux are the result of a reduced energy availability for evaporation. Combined, the reduced energy availability and the *Sphagnum* to feather moss transition produce a 68% reduction in the latent heat flux between a density of 0 and 4 trees per m^2. Incorporating changes to the peatland aerodynamic properties further reduces evaporation; from 0 to 16 W m^{-2} between a tree density of 0 to 1.5 trees per m^2 and remaining more constant at 18 W m^{-2} at densities above 1.5 trees per m^2 (Figure 10a). This reduced evaporation results primarily from an increased subcanopy resistance (Figure 10b; subcanopy resistance). Changes in response to a varying surface roughness are small (Figure 10b; aerodynamic resistance).

[39] The simulated reductions in the latent heat flux with increasing tree densities result from complex interactions and feedbacks between the surface and subsurface energy fluxes (Figure 11a). The surface long-wave radiation reduces substantially with increasing tree density as a consequence of the reduced energy availability and increasing surface resistance. This induces a decrease in the average surface temperature by over 1°C while the sensible heat flux remains approximately constant (the sensible heat flux is on average negative, cooling the surface during the day and warming the surface at night).

[40] The spatial variability in surface fluxes and temperature is strongly dependent on tree density (Figures 11b and 11c). The latent and sensible heat fluxes show the greatest variability between a tree density of 1–2 trees per m^2. This is associated within the transition from a *Sphagnum* to feather moss dominated surface. During this transition there is a strong spatial variation in the surface resistance and thus

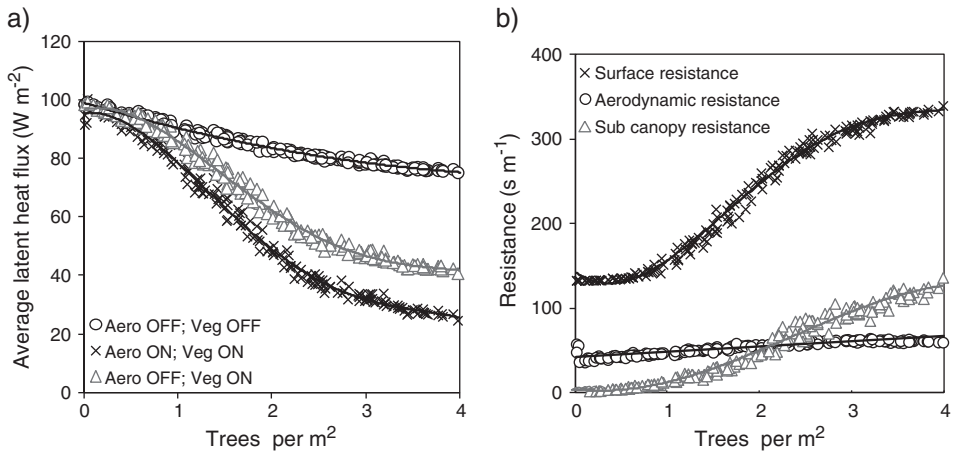

Figure 10. (a) Average latent heat flux simulated with an increasing density of randomly distributed trees with the BETA "aerodynamic" and "vegetation" submodels switch off and on. (b) The surface resistance, aerodynamic resistance, and subcanopy resistance simulated with the "aerodynamic" and "vegetation" submodels switched on.

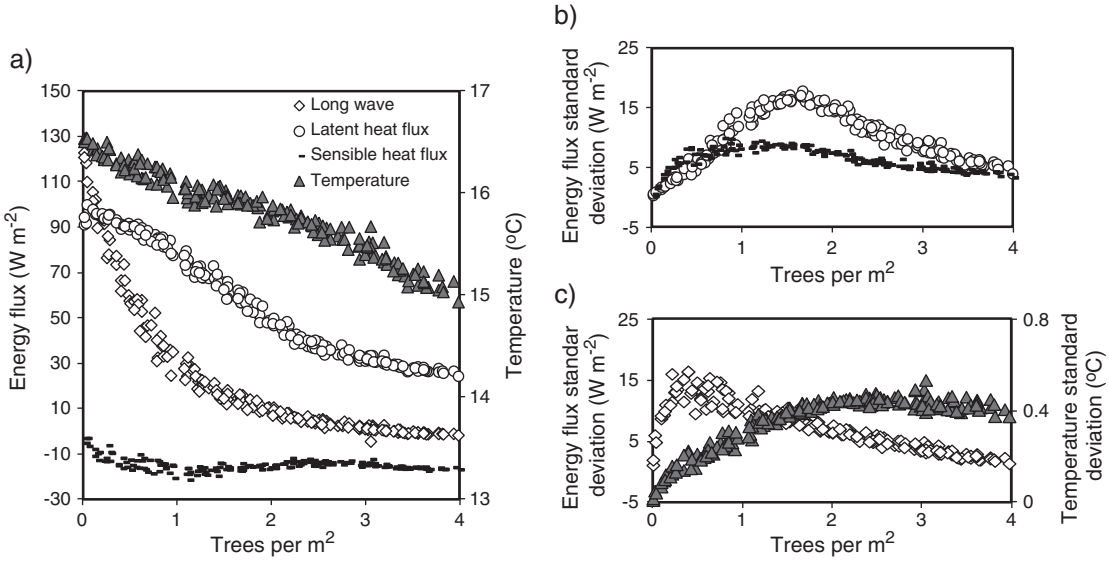

Figure 11. (a) Average long-wave radiation, latent heat flux, sensible heat flux and peat surface temperature with an increasing density of randomly distributed trees. (b) Standard deviation of average latent heat flux, sensible heat flux, (c) long-wave radiation and soil temperature across the 10×10 m simulation area with increasing tree density.

a resultant strong variation in turbulent fluxes. In comparison, spatial variations in the long-wave radiation are controlled more strongly by available energy. At very low tree densities the energy availability is relatively uniform and the spatial variation in long-wave radiation is low. The spatial variability in the available energy and long-wave radiation increases substantially with a small increase in the tree density. Subsequently, as the canopy becomes enclosed, the available energy becomes more spatially uniform and the variability in the long-wave radiation reduces.

4.5. Transpiration vs. Evaporation

[41] Average transpiration increases linearly with increasing tree density, up to 105 W m^{-2} at a density of 4 trees per m^2 (Figure 12). The increasing transpiration and reducing evaporation produces a nonlinear response of the peatland evapotranspiration to increasing tree densities. Up to tree densities of 2.5 trees per m^2, the decrease in evaporation counteracts the associated transpiration increase and evapotranspiration remains approximately constant. Above a density of 2.5 trees per m^2, the decrease in evaporation per unit increase in tree density decreases and, as a result, the total evapotranspiration from the peatland increases from 100 to 130 W m^{-2}.

4.6. Model Simulation: Statistical Tree Generation

[42] Within the Athabasca bog, trees are not randomly distributed, but show significant clustering ($p < 0.01$; $z = -6.85$, mean distance = 0.65 m, expected mean distance = 0.81 m; Moran's *I*). Tree spatial organization provides an important control on the latent heat flux for a given tree density. Figure 13 compares the average latent heat flux for tree distributions generated from the statistical tree generation model at three different tree densities (0.5, 1.5, and 2.5 trees per m^2). The nearest neighbor distance represents the extent of clustering for a given tree density and is equal to the average distance between each tree within the simulation area and its associated

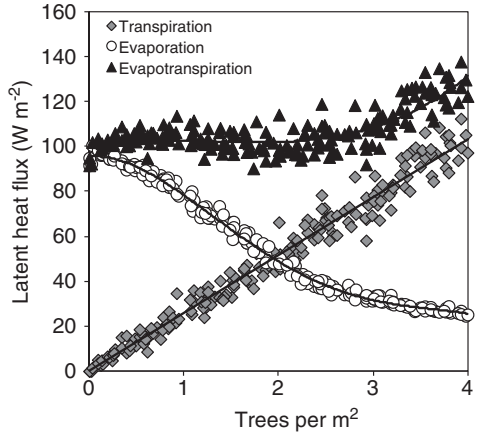

Figure 12. Comparison of simulated evaporation, transpiration, and evapotranspiration with increasing tree density. Solid lines represent linear ($r^2 = 0.97$), fourth order ($r^2 = 0.99$), and third order ($r^2 = 0.78$) regression for the transpiration, evaporation and evapotranspiration simulations, respectively.

nearest neighbor (m). The sensitivity of the latent heat flux to the nearest neighbor distance varies strongly with tree density. At a density of 0.5 trees per m^2, the average latent heat flux varies by 7 W m^{-2} over the range of simulated nearest neighbor distances; decreasing by 1.0 W m^{-2} for every 0.1 m increase in nearest neighbor distance. At a density of 1.5 and 2.5 trees per m^2, this increases to 5.8 and 9.1 W m^{-2}, respectively.

5. Discussion

5.1. Subcanopy Evapotranspiration

[43] Our results confirm the higher rate of evapotranspiration from *Sphagnum* compared to feather mosses. This is due primarily to differences in plant physiology. In *Sphagnum*,

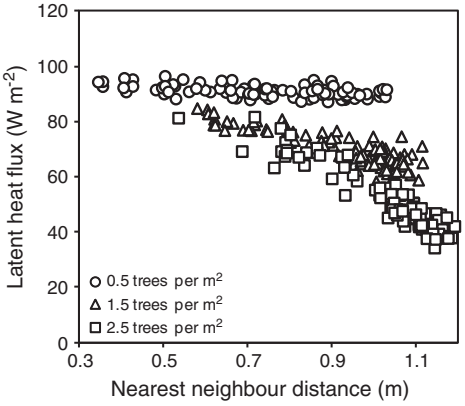

Figure 13. Average latent heat flux from 10 × 10 m simulation area with nearest neighbor distance for different tree densities.

water is transported by an external wicking system and adsorption along the stem and leaf surfaces [*Nichols and Brown*, 1980]. Such a developed transport mechanism is lacking within feather moss [*Callaghan et al*., 1978]. Tree removal significantly increased evapotranspiration from *Sphagnum* plots. The increased evaporative demand that results from the increased direct and diffuse solar radiation at the peat surface was not minimized by an associated increase in surface resistance [*Bond-lamberty et al*., 2011]. Further research is required to characterize peatland vadose zone hydrology and to quantify the regulation of evaporation by the surface resistance effectively within BETA. However, these measurements indicate that under the experimental conditions, a constant surface resistance within *Sphagnum* communities during model simulations with a constant water table depth will provide a reasonable approximation of the ecohydrological behavior of peatland evaporation and its response to varying canopy densities. This important negative feedback mechanism, which will reduce evaporation under increased evaporative demand, should be borne in mind though within the subsequent discussion.

5.2. Boreal Ecohydrology Tree Algorithm Simulations

[44] Boreal Ecohydrology Tree Algorithm provides a reasonable approximation of measured view factors within the 30 × 30 m evaluation plot. With the additional evaluation of the separate components of BETA, notably of the HIP-3D model [*Kettridge and Baird*, 2008, 2010] and the radiation model of *Essery et al*. [2008], we are confident that BETA is providing a reasonable approximation of the simulated ecohydrological processes. Our simulations highlight the complex interactions and feedback that control the response of evaporation to different tree densities. Each feedback incorporated within the BETA model (radiation, vegetation, aerodynamic) provides an important modification of the evaporative losses and must be represented fully to quantify the magnitude of the response. Assuming a random tree distribution, the radiation and aerodynamics impacts on evaporation are largely linear, with rates of evaporation decreasing with increasing tree density. In comparison, the vegetation response is strongly nonlinear.

[45] The spatial organization of trees has been shown to provide a key control on evaporation, modifying the predicted evaporative losses calculated assuming a random tree distribution. This is important because self-organization and patterning is a characteristic of a wide range of peatland environments. To characterize current landscape evapotranspiration losses, knowledge of the spatial organization of trees and the processes that regulate this spatial organization is therefore essential [*Harper et al*., 2006]. For example, stems may show strong clustering in peatland as a result of layering; the generation and rooting of black spruce from the lower branches of a parent tree. The number of "trees" above ground per m^2 may be high within such a peatland. However, because of the strong clustering, evaporation losses will be high for the given stem density.

[46] Increasing tree densities or diameters are commonly seen in response to peatland drainage and thus potentially in response to drying under a changing climate [*Hillman and Roberts*, 2006; *Turetsky et al*., 2011]. Although our analysis interprets the evapotranspiration from different peatlands with different tree densities, we can use this analysis to interpret what the impact of increased tree density may be on evaporation in response to disturbance. However, it is important to recognize that this represents a small component of the complex response of peatland to disturbance (notably the impact of short-term feedback mechanisms need to be integrated within this response). Furthermore, our simulations assume that the subcanopy vegetation cover is in equilibrium with the given tree density. When the ecosystem responds to a disturbance, a lag in the recolonization of the peat surface by feather moss or *Sphagnum* may be evident.

[47] With rates of evapotranspiration varying nonlinearly with tree densities, evapotranspiration shows a nonlinear medium term ecohydrological feedback to drying. Initially, evapotranspiration remains relatively constant with increasing tree densities providing only a small modification to the peatland water balance. Such a shift in the source of evapotranspiration will provide an important modification to peatland vadose zone hydrology, with water being drawn from plant roots rather than from the peatland surface. As a result, the peatland will become vulnerable to drying during extreme drought conditions because peatland evapotranspiration may not be regulated by strong short-term negative ecohydrological feedbacks. Evaporation shows a strong negative feedback response to drying. As the peatland dries, tensions in the near surface peat increase, substantially reducing evaporation losses [*Kettridge et al*., 2012; *Bond-lamberty et al*., 2011], maintaining high peatland water table positions. In comparison, transpiration may have a weaker negative feedback response to drying if black spruce trees are able to extract water that is stored under high tensions (negative soil water potentials) within the peatland [*Angstmann et al*., 2012].

5.3. Implications of Research

[48] This research develops our understanding of the hydrological response of forested peatlands to disturbance in the medium term and the associated vulnerability of their carbon store. Simulations indicate that an increase in tree density within a forested peatland will not increase evapotranspiration losses (except at very high tree densities). As a result, drying due to drainage or increased evaporative demand (under future climatic conditions) will not be exacerbated by the afforestation that may result [*Pellerine and*

Lavoie, 2003]. The stability of this important component of the water balance will limit modifications to the hydrology of both the peatland and the wider region in response to disturbance; the impact severity of a disturbance will be less than if a strong positive feedback response was evident. Furthermore, with high water table levels maintained, alterations to the carbon fluxes will also be comparatively smaller. Rates of peat decomposition depend strongly on the depth of the anaerobic zone [*Moore and Dalva*, 2006] and carbon sequestration is controlled by the availability of water within the near surface [*Thompson and Waddington*, 2008]. However, to fully determine the system response, this knowledge must be incorporated into models that account for the broad array of ecohydrological feedback mechanisms that regulate the ecohydrological and biogeochemical response of peatlands to disturbance.

5.4. Future Developments

[49] Although our simulations account for many of the key feedback mechanisms that regulate the response of evaporation to increased tree densities, further research is required to better characterize the ecohydrological function of forested peatlands to improve our understanding of this key medium-term ecohydrological feedback mechanisms.

[50] Developments are required to better account for the effect of within tree spatial variations in the foliage area volume density on the direct and diffuse radiation received at the peat surface. Our research highlights that the light transmittance per unit path length decreases away from the central portion of the tree. This strongly suggests that the canopy is not uniformly distributed throughout a given volume, but is instead more clustered around the tree trunk. Although the current parameterization of BETA provides a good approximation of the bulk impact of each tree, a more detailed understanding of the distributed nature of the canopy may offer an improved understanding of tree interactions on available energy and light.

[51] Medium-term shifts in subcanopy species (several decades), from *Sphagnum* to feather moss, provide an important control on the hydrological response of peatlands to increasing tree densities. Such a range in subcanopy species composition is evident in peatlands across northern/central Alberta, with open *Sphagnum* dominated peatlands and enclosed (high tree density) feather moss peatlands being widely observed. However, peatlands with a high tree density but low feather moss cover are also evident. For example, *Wieder et al*. [2009] showed that *Sphagnum fuscum* remained dominant at tree densities up to 3.7 trees per m^2. This indicates an additional control on the *Sphagnum*-feather moss transition within peatland ecosystems. Hydrology (water table depth) was shown by *Bisbee et al*. [2001] to influence the ability of feather moss to out-compete *Sphagnum*; *Sphagnum* being more dominant under wetter hydrological conditions. Furthermore, variations in peat depth also impact the faction of *Sphagnum* and feather moss. This is likely controlled by the impact of pore water pH on feather moss growth as indicated by long-term studies simulating acid precipitation onto Canadian boreal forests [*Hutchinson and Scott*, 1988]. Currently, BETA simulations do not account for the variation in the *Sphagnum*-feather moss transition to changing hydrological conditions or pH. BETA does not currently incorporate plant water relations. However, one could see how the dampened response of the *Sphagnum*-feather moss transition within wetter ecosystems could limit feather moss establishment and maintain lower surface resistance at high tree densities. Incorporation of the water balance of specific peatlands within BETA, with an improved understanding of the hydrological controls on the *Sphagnum*-feather moss transition, could better account for the observed variation in peatland subcanopy species across the subhumid boreal plain and shield of western Canada.

[52] Boreal Ecohydrology Tree Algorithm accounts for shifts in the subcanopy species between *Sphagnum* and feather moss in response to light availability at the peat surface. This provides a very simplified representation of the complex response of peatland vegetation communities to changing light, hydrology, and nutrient conditions to disturbance [*Miller*, 2011]. Further work is required to improve our understanding of the ecohydrological response of these vegetation communities and to encompass this knowledge within the process-based modeling framework to project the future peatland ecohydrological response to disturbance.

[53] A simple representation of black spruce transpiration was incorporated to provide a broad comparison of evaporation and transpiration rates under a range of tree densities. Although this provides an initial characterization of the potential response of the peatland to increasing tree density, black spruce transpiration cannot be solely related to sap wood fraction and vapor pressure deficit. Transpiration will vary with tree age, peatland hydrological conditions/drainage [*Angstmann et al*., 2012], nutrient, and light availability. To provide a more detailed representation of the ecosystem evapotranspiration, such effects within the subcanopy may need to be incorporated. In addition, interception will also increase under higher tree densities, further counteracting increased rates of transpiration.

6. Conclusion

[54] We have simulated the control of tree density on peatland evaporation. With an increasing tree density, evaporation is decreased due to the reduced energy available at the peat surface and the increased subcanopy resistance. Short-term changes in peat surface resistance within a vegetation community do not counteract these differences, with evaporation increasing significantly and surface resistance varying insignificantly between shaded and unshaded regions. In addition, the reduced light availability at tree densities greater than one tree per m^2 enables feather moss to out-compete *Sphagnum*. Because of the higher surface resistance of feather moss, this increases the peatland surface resistance, producing a strong nonlinear reduction in evaporation.

[55] The reduction in evaporation with increasing tree densities is strongly modified by tree spatial organization. At higher tree densities, clustering limits reductions in evaporation for a given stand density. We have focused on the subcanopy response to varying tree densities and spatial arrangements. However, comparison of evaporation losses simulated by BETA and transpiration losses estimated from a simple transpiration model suggests that evaporation

reductions in response to an increased tree density are approximately equal to the associated increase transpiration (up to densities of 2.5 trees per m^2). As a result, rates of evapotranspiration are potentially insensitive to tree densities, with peatlands maintaining saturated conditions and a resilient carbon store with increased transpiration fluxes.

[56] **Acknowledgments**. This research was funded by a Natural Science and Engineering Council (NSERC) of Canada Discovery Grant and Discovery Accelerator Supplement to JMW as well as a NSERC Strategic Project Grant to JMW and MRT. We thank Richard Essery for providing a copy of the radiative transfer model and Dan Johnston for providing dry foliage mass data for black spruce trees. We would also like to thank Steve Baisley, Jenna Falk, and Rachel Humphrey for field assistance, Michelle Low for data analysis and Niko Yiannakoulias for helpful discussions with this research.

References

Abtew, W., J. M. Gregory, and J. Borreli (1989), Wind profile: estimation of displacement height and aerodynamic roughness, *Transactions of the ASAE*, *32*, 521–527.

Angstmann, J. L., B. E. Ewers, and H. Kwon (2012), Size-mediated tree transpiration along soil drainage gradients in a boreal black spruce forest wildfire chronosequence, *Tree Physiol.*, *32*, 599–611, doi:10.1093/treephys/tps021.

Baird, A. J., P. Morris, and L. R. Belyea (2012), The DigiBog model of peatland development 1: rationale, conceptual model, and hydrological basis, *Ecohydrology*, *5*, 242–255, doi:10.1002/eco.230.

Belyea, L. R. (2009), Nonlinear dynamics of peatlands and potential feedbacks on the climate system, in Carbon Cycling in Northern Peatlands, Geophysical Monograph Series 184, pp. 5–18, American Geophysical Union, Washington, D.C.

Benscoter, B. W., R. K. Wieder, and D. H. Vitt (2005), Linking microtopography with post-fire succession in bogs, *J. Veg. Sci.*, *16*, 453–460, doi:10.1139/X05-115.

Bisbee, K. E., S. T. Gower, J. M. Norman, and E. V. Nordheim (2001), Environmental controls on ground cover species composition and productivity in a boreal black spruce forest, *Oecologia*, *129*, 261–270.

Bond-lamberty, B., C. Wang, S. T. Gower, and J. Norman (2002), Leaf area dynamics of a boreal black spruce fire chronosequence, *Tree Physiol.*, *22*, 993–1001.

Bond-lamberty, B., S. T. Gower, B. Amiro, and B. E. Ewers (2011), Measurement and modelling of bryophyte evaporation in a boreal forest chronosequence, *Ecohydrology*, *35*, 26–35, doi:10.1002/eco.

Brock, B., and N. Arnold (2000), Technical communication – a spreadsheet-based (Microsoft Excel) point surface energy balance model for glacier and snow melt studies, *Earth Surf. Land.*, *25*, 649–658.

Brown, S. M., R. M. Petrone, C. Mendoza, and K. J. Devito (2010), Surface vegetation controls on evapotranspiration from a sub-humid Western Boreal Plain wetland, *Hydrol. Process.*, *24*, 1072–1085, doi:10.1002/hyp.7569.

Callaghan, T. V., N. J. Collins, and C. H. Callaghan (1978), Photosynthesis, growth and reproduction of *Hylocomium splendens* and *Polytrichum commune* in Swedish Lapland, *Oikos*, *31*, 73–88.

Cionco, R. M. (1983), On the coupling of canopy flow to ambient flow for a variety of vegetation types and densities, *Bound.-Lay. Meteorol.*, *26*, 325–335.

Daamen, C. C., and L. P. Simmonds (1996), Measurement of evaporation from bare soil and its estimation using surface resistance, *Water Resour. Res.*, *32*, 1393–1402.

Ecoregions Working Group (1989), Ecological Land Classification, Series No. 23, Sustainable Development Branch, Canadian Wildlife Service, Conservation and Protection, Environment Canada, Ottawa, Canada, 119.

Essery, R., P. Bunting, J. Hardy, T. Link, D. Marks, R. Melloh, J. Pomeroy, A. Rowlands, and N. Rutter (2008), Radiative Transfer Modeling of a Coniferous Canopy Characterized by Airborne Remote Sensing, *J. Hydrometeorol.*, *9*, 228–241, doi:10.1175/2007JHM870.1.

Frazer, G. W., C. D. Canham, and K. P. Lertzman (2001), Gap Light Analyzer, Version 2.0., *Bulletin of the Ecological Society America*, *81*, 191–197.

Goudriaan, J. (1977), *Crop Micrometeorology: A Simulation Study*, 257 pp., Pudoc, Wageningen, Netherlands.

Harper, K. A., Y. Bereron, P. Drapeau, S. Gauthier, and L. De Grandpre (2006), Changes in spatial patten of trees and snags during structural development in *Picea mariana* boreal forests, *J. Veg. Sci.*, *17*, 625–636, doi:10.1111/j.1654-1103.2006.tb02486.x.

Heijmans, M. M. P. D., W. J. Arp, and F. S. C. Iii (2004), Carbon dioxide and water vapour exchange from understory species in boreal forest, *Agr. Forest. Meteorol.*, *123*, 135–147, doi:10.1016/j.agrformet.2003.12.006.

Hillman, G. R., and J. J. Roberts (2006), Early growth response in trees following peatland drainage, *Information Report NOR-X-408*, Natural Resources Canada., Canadian Forestry Service, Northern Forestry Centre, Edmonton, Canada.

Hutchinson, T. C., and M. G. Scott (1988) The response of the feather moss Pleurozium schreberi, to 5 years of simualated acid precipitation in the Canadian boreal forest, *Can. J. Bot.*, *66*, 82–88.

Johnston, D. C. (2012), Quantifying the fuel load, fuel structure and fire behavior of forested bogs and blowdown, M.S. thesis, Faculty of Forestry, University of Toronto, Toronto, Ontario, Canada.

Kettridge, N., and A. Baird (2006), A new approach to measuring the aerodynamic resistance to evaporation within a northern peatland using a modified Bellani plate atmometer, *Hydrol. Process.*, *20*, 4249–4258, doi:10.1002/hyp.

Kettridge, N., and A. J. Baird (2007), In situ measurements of the thermal properties of a northern peatland: Implications for peatland temperature models, *J. Geophys. Res.*, *112*, F02019, doi:10.1029/2006JF000655.

Kettridge, N., and A. J. Baird (2008), Modelling soil temperatures in northern peatlands, *Eur. J. Soil Sci.*, *59*, 327–338, doi:2389.2007.01000.x.

Kettridge, N., and A. J. Baird (2010), The development and application of a 3-D soil temperature model of hummock hollow complexes in northern peatlands, *J. Geophys. Res.*, *115*, G03009, doi:10.1029/2009JG001068.

Kettridge, N., D. K. Thompson, and J. M. Waddington (2012), Impact of wildfire on the thermal behavior of northern peatlands: Observations and model simulations, *J. Geophys. Res.-Biogeosci.*, *117*, G02014, doi:10.1029/2011JG001910.

Lafleur P. M., and C. P. Schreader (1994), Water loss from the floor of a sub-arctic forest, *Arctic Alpine Research*, *26*, 152–158.

Lieffers, V. J., and S. E. Macdonald (1990), Growth and foliar nutrient status of black spruce and tamarack in relation to depth of water table in some Alberta peatlands, *Can. J. Forest Res.*, *20*, 805–809.

MacDonald, S. E., and F. Yin (1999), Factors influencing size inequality in peatland black spruce and tamarack evidence from post drainage release growth, *J. Ecol.*, *87*, 404–412.

McCarter, C. P. R., and J. S. Price (2012), Ecohydrology of Sphagnum moss hummocks: mechanisms of capitula water supply and simulated effects of evaporation, *Ecohydrology*, early view, doi:10.1002/eco.1313.

McLeod, M. K., H. Daniel, R. Faulkner, and R. Murison (2004), Evaluation of an enclosed portable chamber to measure crop and pasture actual evapotranspiration at small scale, *Agr. Water Manage.*, *67*, 15–34, doi:10.1016/j.agwat.2003.12.006.

Miller, C. A. (2011), The effect of long-term drainage on plant community composition, Biomass, and productivity in boreal continental peatlands, M.S. thesis, Department of Integrative Biology, The University of Guelph, Guelph, Ontario, Canada.

Mölder, M., and E. Kellner (2002), Excess resistance of bog surfaces in central Sweden, *Agr. Forest. Meteorol.*, *112*, 23–30, doi:10.1016/S0168-1923(02)00043-6.

Moore, T., and D. Dalva (2006), The influence of temperature and water table position on carbon dioxide and methane emissions from laboratory columns of peatland soils, *Eur. J. Soil Sci.*, *44*, 651–664, doi:10.1111/j.1365-2389.1993.tb02330.x.

Morris, P., A. J. Baird, and L. R. Belyea (2012), The DigiBog model of peatland development 2: ecohydrological simulations in 2-D, *Ecohydrology*, *5*, 256–268, doi:10.1002/eco.229.

Nichols, D. S., and J. M. Brown (1980), Evaporation from a *Sphagnum* moss surface, *J. Hydrol.*, *48*, 289–302.

Niu, G.-Y., and Z.-L. Yang (2004), Effects of vegetation canopy processes on snow surface energy and mass balances, *J. Geophys. Res.*, *109*, D23111, doi:10.1029/2004JD004884.

Oke, T. R. (1987), Boundary Layer Climates, Routledge, New York.

Oren, R., R. Zimmerman, and J. Terbough (1996), Transpiration in upper Amazonian floodplain and upland forests in response to drought-breaking rains, *Ecology*, *77*, 968–973.

Pellerine S., and C. Lavoie (2003), Reconstructing the recent dynamics of mires using a multitechnique approach, *J. Ecol.*, *91*, 1008–1021, doi:10.1046/j.1365-2745.2003.00834.x.

Philip, J. R. (1957), Evaporation, and moisture and heat fields in the soil, *J. Meteorol.*, *14*, 354–366.

Rowe, J. S. (1959), Forest regions of Canada, *Canadian Department North Affairs and National Resources, Forest Branch Bulletin*, *123*, 1–71.

Schneider, C. A., W. S. Rasband, and K. W. Eliceiri (2012), NIH Image to ImageJ: 25 years of image analysis, *Nat. Methods*, *9*, 671–675, doi:10.1038/nmeth.2089.

Stannard, D. I. (1988), Use of a Hemispherical Chamber for Measurement of Evapotranspiration, *Open-File Report 88–452*, United State Geological Survey, Denver, CO.

Strack, M., E. Kellner, and J. M. Waddington (2006), Effect of entrapped gas on peatland surface level fluctuations, *Hydrol. Process.*, *20*, 3611–3622, doi:10.1002/hyp.

Tarnocai, C., J. G. Canadell, E. A. G. Schuur, P. Kuhry, G. Mazhitova, and S. Zimov (2009), Soil organic carbon pools in the northern circumpolar permafrost region, *Global Biogeochem. Cy.*, *23*, GB2023, doi:10.1029/2008GB003327.

Thompson, D. K. (2012), Wildfire impacts on peatland ecohydrology, PhD thesis, School of Geogr. and Earth Sci., McMaster Univ., Hamilton, Ontario, Canada.

Thompson, D. K., and J. M. Waddington (2008), Sphagnum under pressure: towards an ecohydrological approach to examining *Sphagnum* productivity, *Ecohydrology*, *1*, 299–308, doi:10.1002/eco.

Turetsky, M. R., W. F. Donahue, and B. W. Benscoter (2011), Experimental drying intensifies burning and carbon losses in a northern peatland, *Nat. Commun.*, *2*, 514, doi:10.1038/ncomms1523.

Turunen, J., E. Tomppo, K. Tolonen, and A. Reinikainen (2002), Estimating carbon accumulation rates of undrained mires in Finland–application to boreal and subarctic regions, *The Holocene*, *12*, 69–80, doi:10.1191/0959683602hl522rp.

Van de Griend, A. A., and M. Owe (1994), Bare soil surface resistance to evaporation by vapor diffusion under semiarid conditions, *Water Resour. Res.*, *30*, 181.

Wieder, R. K., K. D. Scott, K. Kamminga, M. A. Vile, D. H. Vitt, T. Bone, B. Xu, B. W. Benscoter, and J. Bhatti (2009), Post-fire carbon balance in boreal bogs of Alberta Canada, *Glob. Chang. Biol.*, *15*, 63–81, doi:10.1111/j.1365-2486.2008.01756.x.